

# Making a splash with water repellency

Cyril Duez<sup>†</sup>, Christophe Ybert<sup>†</sup>, Christophe Clanet<sup>‡</sup>, Lydéric Bocquet<sup>†\*</sup>

<sup>†</sup> Laboratoire PMCN, Université Lyon 1, UMR CNRS 5586, 69622 Villeurbanne, France

<sup>‡</sup> IRPHE, UMR CNRS 6594, 13384 Marseille, France

PACS numbers:

A 'splash' is usually heard when a solid body enters water at large velocity. This phenomena originates from the formation of an air cavity resulting from the complex transient dynamics of the free interface during the impact. The classical picture of impacts on free surfaces relies solely on fluid inertia, arguing that surface properties and viscous effects are negligible at sufficiently large velocities. In strong contrast to this large-scale hydrodynamic viewpoint, we demonstrate in this study that the wettability of the impacting body is a key factor in determining the degree of splashing. This unexpected result is illustrated in Fig.1: a large cavity is evident for an impacting hydrophobic sphere (1.b), contrasting with the hydrophilic sphere's impact under the very same conditions (1.a). This unforeseen fact is furthermore embodied in the dependence of the threshold velocity for air entrainment on the contact angle of the impacting body, as well as on the ratio between the surface tension and fluid viscosity, thereby defining a critical capillary velocity. As a paradigm, we show that superhydrophobic impacters make a big 'splash' for any impact velocity. This novel understanding provides a new perspective for impacts on free surfaces, and reveals that modifications of the detailed nature of the surface – involving physico-chemical aspects at the nanometric scales – provide an efficient and versatile strategy for controlling the water entry of solid bodies at high velocity.

The first systematic study of splashes was published more than one century ago by Worthington<sup>1</sup>, who used high speed photography to examine impacts of drops and solid bodies on a liquid surface. In the recent years, there has been a resurgence in interest in the physics of impact, thanks in particular to the development of rapid video imaging. And new perspectives have emerged, showing that unforeseen mechanisms play a central role in impact: to cite a few, the inhibition of droplet rebound by adding tiny amounts of polymers<sup>2</sup>, the complex deformation dynamics of a rebounding drop<sup>3</sup>, and the unexpected role of ambient air on drop splashing<sup>4,5</sup>. We consider in this study the situation of a solid body impacting a gas-liquid interface. This situation is obviously relevant for many naval applications, such as ship slamming and air to sea weapons, and for any industrial coating process which involves the dipping of a solid object in a liquid bath (where air entrainment is to be avoided). The traditional de-

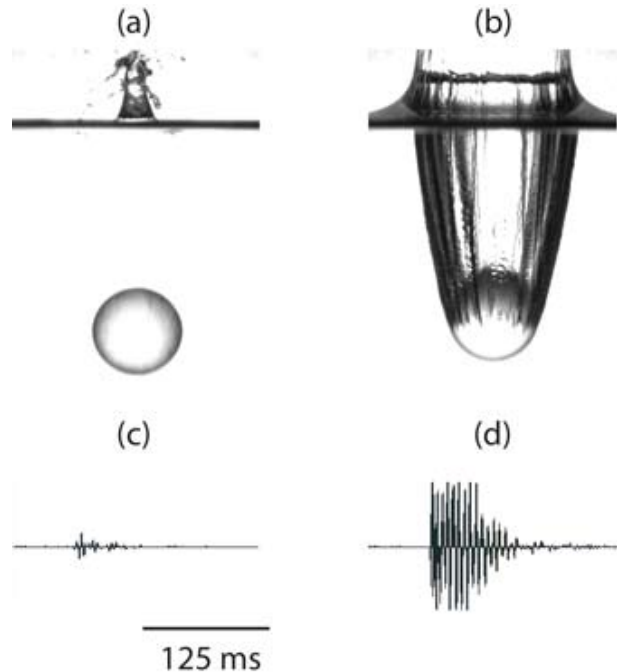


FIG. 1: *Top*: Photographs of the impact of two spheres differing only in wettability via a nanometric coating on their surface: (a) impact of a perfectly wetting sphere, with static contact angle  $\theta_0 \simeq 15^\circ$ ; (b) impact of a hydrophobic sphere with static contact angle  $\theta_0 \simeq 100^\circ$ . The impact velocity was  $5.0 \text{ m.s}^{-1}$  in both cases, corresponding to a  $1.25\text{m}$  height drop. Pictures were taken  $15.5\text{ms}$  (left) and  $15.0\text{ms}$  (right) after impact beginning. *Bottom*: Time-dependent audio recordings of the impacts, as measured by a microphone  $\sim 10 \text{ cm}$  from the impact point, for (c) a hydrophilic and (d) a hydrophobic sphere. The signal is proportional to the acoustic pressure emitted during the impact. Units on the vertical scale are arbitrary (but identical). A big 'splash' is evident for the hydrophobic sphere, while a tiny 'plop' is heard for the hydrophilic one. The sound is associated with the rapid closure of the cavity (not shown).

scription of an impact of a solid body on a free interface follows the footsteps of von Karman and Wagner<sup>6,7</sup>, in which viscosity, surface tension and compressibility effects are neglected<sup>8,9</sup>. This idealized framework is formally justified by the fact that in the situations relevant to impacts, the Reynolds  $Re$  and Weber  $We$  numbers, quantifying the role of inertia versus respectively viscous and capillary effects, are very large. This is precisely the regime of interest in this study:  $Re = \rho U a / \mu_L \gtrsim$

$10^4 - 10^5$  and  $We = \rho U^2 a / \gamma_{LV} \gtrsim 10^3 - 10^4$  (for impacting body diameter  $a$ , velocity  $\bar{U}$ , liquid density  $\rho$ , liquid viscosity  $\mu_L$ , and liquid-vapour surface tension  $\gamma_{LV}$ ). Accordingly, capillarity and viscosity are not expected to play any role in the impact and can be ignored in this description.

Our experimental results contrast with this simple picture. As illustrated in Fig.1, two spheres that only differ by a nanometric coating which modifies wettability exhibit very different impact behavior: a huge air cavity is entrained for the hydrophobic sphere, while no such behavior is observed for the hydrophilic one. However, apart from the static contact angle ( $\theta_0 \simeq 15^\circ$  versus  $\theta_0 \simeq 100^\circ$ ), the spheres are identical in terms of bulk material (glass), diameter, very low surface roughness and impact velocity ( $U = 5\text{m.s}^{-1}$ ). Moreover, during the experiment, a 'splash' is heard for the hydrophobic sphere, while only a tiny 'plop' is produced by the hydrophilic one, as shown in Fig.1 (c-d). This observation raises puzzling questions:

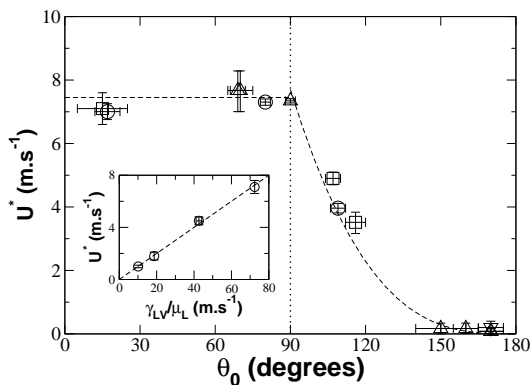


FIG. 2: Threshold velocity  $U^*$  for air entrainment as a function of (advancing) static contact angle  $\theta_0$  of the impacting body. The dashed lines are the theoretical predictions based on relations (1) and (2). The different symbols correspond to different bead diameters:  $\square$  25.4 mm (glass);  $\nabla$  20mm (aluminium);  $\circ$  15mm (glass, steel);  $\triangle$  7mm (aluminium, steel). The beads are covered with various coatings to modify their wettability (see Method section). To focus on wettability as the only surface parameter, only smooth objects have been considered in the present study (see Method section). *Inset*: Dependence of the threshold velocity for a wetting glass sphere (25.4mm) on the ratio  $\gamma_{LV}/\mu_L$ . We used various liquids to explore this dependence: water, isopropanol, ethanol, a water-glycerol mixture (20wt% of glycerol). For these fluids, the contact angle on the sphere surface was always below  $10^\circ$ . The dashed line is a linear prediction  $U^* = \xi \gamma_{LV}/\mu_L$  (with  $\xi \simeq 0.1$ ).

how can a nanometric coating modify large scale hydrodynamics? More generally, how might capillarity affect the flow pattern in the limit of large Weber numbers? To answer these questions, we have first explored the conditions required to create an air cavity, as illustrated in

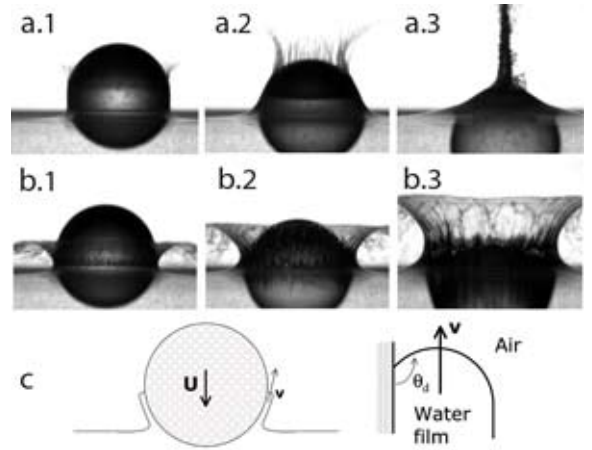


FIG. 3: Detailed chronophotography of impacting spheres with two different wettabilities at the same impact velocity  $U = 5\text{m.s}^{-1}$ : (a.1)-(a.3) hydrophilic sphere (1.4, 2.2 and 3.9 ms after impact start); (b.1)-(b.3) hydrophobic sphere (1.5, 2.4 and 4.0 ms after impact start). For the hydrophilic sphere, the considered impact velocity is below the threshold for air entrainment: the ascending film is shown to follow the sphere and gather at the pole. For the hydrophobic sphere, the impact velocity is above the threshold for air entrainment: the ascending film detaches from the sphere, thereby creating a cavity during the impact. (c) *left* - Sketch of the impact geometry; *right* - magnification of the triple line region.  $\theta_d$  is the dynamic contact angle, which is larger than the static contact angle  $\theta_0$  for a moving triple line (with velocity  $v$ ). The threshold velocity is reached as the contact line is no longer stable, which occurs as  $\theta_d \rightarrow 180^\circ$ .

the above example. By varying the velocity of the impacting body, we have demonstrated that an air cavity is created during an impact only above a threshold velocity,  $U^*$ , typically of a few meters per second. Furthermore this threshold velocity is found to depend on the (advancing) contact angle  $\theta_0$  of the impacting body. The experimental results for  $U^*$  in water are gathered in Fig.2 for spheres with various wettabilities. Going further, we measured the dependence of the threshold velocity  $U^*$  on the liquid properties, by considering impacts on various liquids (with different viscosities and surface tensions) for fixed wettability. As shown in the inset of Fig.2, we found that  $U^*$  is proportional to the capillary velocity, defined as  $\gamma_{LV}/\mu_L$ . To complete this exploration, we verified that the diameter of the impacting sphere does not influence the threshold (see Fig.2), neither gas pressure (varied between 0.1 and 1 atm). To rationalize these results, we zoom in on the detailed dynamics of the impact. An essential characteristic of solid to liquid impacts is that a thin film develops during the impact and climbs up the impacting body<sup>10</sup>. This film is evident in Fig.3 (a.1)-(a.3). However, the film dynamics is seen to strongly differ depending on whether the velocity is below or above the threshold  $U^*$  for air entrainment. For the velocity considered in Fig.3, the hydrophilic sphere is below

the threshold: the film is seen to follow the sphere and closes up at the pole of the sphere (Fig.3 (a.1)-(a.3)). As such, no cavity is created. On the contrary, for the same velocity, the hydrophobic sphere is above threshold and the film is seen to detach from the sphere *before* reaching the pole (Fig.3 (b.1)-(b.3)). The opened aperture left at the top of the sphere then leads to cavity formation and air entrainment. These pictures thus point to the film dynamics as the origin of air entrainment and splash.

We therefore propose an interpretation of these results in terms of contact line stability. The geometry is described in Fig.3(c). The liquid film and triple line move at a velocity  $v$  of  $v \approx \zeta U$ , with  $\zeta \approx 2$  (see<sup>8</sup>). Let us first consider the motion of the film on a hydrophobic sphere. In this case the gas (air) is the wetting phase and the solid surface moves *towards* the non-wetting phase (liquid). This situation corresponds to the prototypical problem of forced (de)wetting, but here with the air replacing the liquid in the role of the wetting phase, see Fig.3c. Since the work of de Gennes<sup>11</sup>, it has been known that a critical speed exists above which the triple line is no longer stable, as the dynamic contact angle  $\theta_d$  goes to  $180^\circ$ <sup>12</sup>. Above this critical speed, the solid will be coated by the wetting phase, here air. A hydrodynamic force balance at the contact line shows that this occurs at a critical capillary number  $Ca^* = \mu v^* / \gamma_{LV}$  obeying  $Ca^* \approx \Theta_0^3 / 9\ell$ , with  $\Theta_0$  the static contact angle as defined with respect to the wetting phase (air) and  $\ell \approx 15 - 20$ , see<sup>11,12</sup>. Using  $\Theta_0 = \pi - \theta_0$ , one gets  $Ca^* \approx (\pi - \theta_0)^3 / 9\ell$ . This classical reasoning, however, neglects dissipation in the non-wetting phase (here water). This assumption is obviously not valid. We have added a liquid viscous contribution in the force balance at the triple line, in the form  $F_L \approx C\mu_L v$  (with  $C \sim 1$ ). This term adds to the classical contribution in the wetting phase corner, here  $F_{air}(v) = \frac{3\mu_{air}\ell}{\pi - \theta_d} v$ , diverging as  $\theta_d \rightarrow 180^\circ$ . Both terms are of the same order of magnitude since  $\alpha = 3\ell\mu_{air} / \mu_L \sim 1$ . Using this new expression for the frictional force, the critical velocity is found to be of the form  $v^* = \frac{g_0}{9\ell} \frac{\gamma_{LV}}{\mu_L} [\pi - \theta_0]^3$ , defining a critical capillary number in terms of the *liquid* viscosity. The numerical prefactor  $g_0$  is typically on the order of  $\sim 5 - 10$ , with a weak dependence on the liquid and gas viscosity. Using  $v = \zeta U$ , one gets eventually the threshold velocity for non-wetting impacters ( $\theta_0 \geq 90^\circ$ ),

$$U^* = \frac{g_0}{9\ell\zeta} \frac{\gamma_{LV}}{\mu_L} [\pi - \theta_0]^3. \quad (1)$$

As shown in Fig.2, this theoretical prediction is in very good agreement with the experimental results with hydrophobic impacters ( $\theta \geq 90^\circ$ ). This mechanism culminates in the superhydrophobic limit, for which the impacting body entrains air for any velocity. Fixing  $\ell = 15$  and  $\zeta = 2$ , experimental results are quantitatively reproduced with  $g_0 \approx 7$  (which corresponds to  $C \simeq 2.9$ ).

The situation of a hydrophilic impacting sphere may be discussed along the same lines. While the contact angle is lower than  $90^\circ$  for small velocities, the dynam-

ical contact angle  $\theta_d$  will increase with the triple line velocity  $v$ . As above, the triple line will disappear as  $\theta_d \rightarrow 180^\circ$ <sup>12</sup>. Unfortunately, no analytical description is available for  $\theta_d(v)$  in this limit when starting from a wetting surface ( $\theta_0 \leq 90^\circ$ ). Nevertheless the physics are qualitatively similar to that described above for the non-wetting surfaces and the dissipation in air, which diverges as  $\theta_d \rightarrow 180^\circ$ , will destabilize the contact line above a threshold velocity. We therefore expect again a critical velocity, scaling as in the previous case like

$$U^* \approx \xi \frac{\gamma_{LV}}{\mu_L}. \quad (2)$$

The prefactor  $\xi$  may depend on the static contact angle  $\theta_0$ . However, since at the threshold for destabilization  $\theta_d^* \sim \pi$  is significantly larger than the static contact angle  $\theta_0$ , we only expect a weak dependence of  $\xi$  on  $\theta_0$ . This point is confirmed experimentally, as shown in Fig.2: in the wetting regime the critical velocity for air entrainment is basically independent of the static contact angle. Moreover changing the fluid fully confirms the linear dependence of  $U^*$  on  $\frac{\gamma_{LV}}{\mu_L}$  as embodied in expression (2) (see Fig.2, inset). Comparison with experimental results suggests  $\xi \approx 0.1$  (see Fig.2, inset).

We finish with a short discussion on the 'splashing' sound, which can be heard above threshold (see Fig.1). The sound arises from the rapid closure of the cavity as it pinches off. These dynamics are gravity-driven so that the closure time is typically  $\tau \sim \sqrt{a/g}$ , with  $a$  the size of the impacting object and  $g$  the gravitational constant<sup>13,14</sup>. For a centimeter body,  $\tau \sim 100$ ms, in full agreement with the recordings shown in Fig.1 (to compare with the impact time  $a/U \sim 5$ ms in this case). As we confirmed independently, the splash duration and amplitude are therefore independent of the impact velocity!

To conclude, our results give a new perspective on impacts in liquids, by pointing to the unexpected role of surface properties. Air entrainment is best inhibited by using clean and wetting surfaces. Hydrophobic objects make a splash.

## Methods

### Surface treatments to control wettability

We use spheres made of glass, steel and aluminium, with diameters varying between 7 and 25.4mm.

Wetting glass beads ( $\theta_0 \simeq 15 - 20^\circ$ ) are obtained by immersion during 40 min in a piranha solution [1 vol.  $H_2O_2$ , 2 vol.  $H_2SO_4$ ], then rinsed using deionized water and isopropanol, and eventually heated at  $110^\circ C$  for 20 min.

Hydrophobic glass beads ( $\theta_0 \simeq 100 - 120^\circ$ ) are obtained by grafting silane chains on the surface. We chose grafting of octyltriethoxysilane ( $105^\circ$ ) or perfluorooctyltrichlorosilane ( $110 - 120^\circ$ ) in the gas phase (by pumping

in a closed vessel), for 15 hours at ambient temperature. After silanisation, the beads are rinsed with isopropanol, dried and heated at 90° C during one hour.

Superhydrophobic aluminium beads ( $\theta_0 \simeq 150 - 170^\circ$ ) are obtained following the chemical protocol proposed by Qian and Zhen<sup>15</sup>. The aluminium beads are first plunged in an aqueous solution of chlorhydric and fluorhydric acids for 15 s. Then a silane coating (perfluorooctyltriethoxysilane) is grafted on the beads by silanisation in the liquid phase at ambient temperature for one hour and then heated at 130°C for one hour. This protocol works only for pure aluminium and we therefore used 1050 Al.

The contact angle on the steel beads is  $\theta_0 \sim 80 - 90^\circ$ , obtained after cleaning with deionized water with detergent, and then with isopropanol. An AFM topographic scan of the beads' surface shows that for the beads considered in this study, the peak-to-peak roughness was smaller than 100 nanometers (with a rms roughness of  $\sim 5\text{nm}$  for a  $10\mu\text{m} \times 10\mu\text{m}$  scan). Larger scale roughness was probed with a profilometer (Tencor Instruments) with a  $5\mu\text{m}$  tip showing less than 20nm rms deviation over a millimeter scan. For the superhydrophobic coatings, we have shown moreover in a previous work using AFM measurements that the liquid interface on the coatings is very smooth with a peak-to-peak roughness in the hundreds of nanometers range<sup>16</sup>.

#### Impact experimental setup and protocole

The beads are released from rest at varying heights above a transparent box containing the liquid. The impact is recorded using a high speed video camera (Mikrotron) at a frame rate of  $\sim 1000$  fps. The impact speed is determined from the movie. Before each release, the beads are cleaned by rinsing with isopropanol, dried using azote and heated at 110°C for 20 min for a complete drying. We left the beads cooling to ambient temperature before impact. Most of our experiments are conducted with water, but to study the effect of fluid characteristics (viscosity, surface tension) we use ethanol, isopropanol, and a water-glycerol mixture (20wt% of glycerol) to vary the viscosity. The contact angle on the bare glass beads with these fluids was always smaller than  $10^\circ$ . The viscosity of the water-glycerol mixture was measured before and after each impact using a Ubbelohde viscometer. Values for the surface tensions were taken from litterature.

**Acknowledgements** : This project was supported by the French Ministry of Defense, via DGA. L.B. would like to thank Jean-François Pinton for discussions on the subject and D. Huang for a careful reading of the manuscript. The authors thanks Sébastien Manneville for kindly lending us the high speed video system and Marie-Charlotte Audry for the AFM scans.

**Conflict of interest** : the authors declare that they have no competing financial interests.

**Correspondance** and requests for materials should be addressed to L. B. (lyderic.bocquet@univ-lyon1.fr)

---

\* Electronic address: lyderic.bocquet@univ-lyon1.fr

<sup>1</sup> Worthington, A.M., Cole, R.S., Impact with a liquid surface studied by the aid of instantaneous photography II, *Phil. Trans. Roy. Soc. London A* **194** 175-199 (1900)

<sup>2</sup> Bergeron, V., Bonn, D., Martin, J.-Y., Vovelle, L., Controlling droplet deposition with polymer additives, *Nature* **405** 772-775 (2000)

<sup>3</sup> D. Richard, C. Clanet, D. Quéré, Contact time of a bouncing drop, *Nature* **417** 811 (2002)

<sup>4</sup> Xu, L. , Zhang, W. W., Nagel, S. R., Drop splashing on a dry smooth surface, *Phys. Rev. Lett.* **94**, 184505 (2005).

<sup>5</sup> Quéré, D., Impact on Everest, *Nature*, **435** 1168 (2005).

<sup>6</sup> von Kármán, T., The impact on seaplane floats during landing, *NACA TN* **321** (1929).

<sup>7</sup> Wagner, H., Phenomena associated with impacts and sliding on liquid surfaces, *Zeitschrift für Angewandte Mathematik und Mechanik*, **12** 193-215 (1932)

<sup>8</sup> James Oliver, *Water entry and related problems*, PhD Thesis, Oxford University (2002)

<sup>9</sup> S. Howison, J.R Ockendon, and J.M. Oliver Oblique slamming, planing and skimming, *Journal of Engineering*

*Mathematics*, **48** (3-4). pp. 321-337 (2004)

<sup>10</sup> Korobkin, A.A., Pukhnachov, V.V., Initial stages of water impact, *Ann. Rev. Fluid Mech.* **20** 159-185 (1988)

<sup>11</sup> de Gennes, P.-G. , Brochard-Wyart, F. , Quéré, D., *Gouttes, bulles, perles et ondes* (Belin, 2005).

<sup>12</sup> Eggers, J., Hydrodynamic theory of forced dewetting, *Phys. Rev. Lett.* **93** 094502 (2004).

<sup>13</sup> Glasheen, J.W., McMahon, T.A., Vertical water entry of disks at low Froude numbers, *Phys. Fluids*, **8** 2078-2083 (1996).

<sup>14</sup> Duclaux, V., Caillé, F., Duez, C., Ybert, C., Bocquet, L., Clanet, C., Dynamics of transient cavities, submitted to *J. Fluid Mech.* (2006).

<sup>15</sup> Qian, B., Shen, Z., Fabrication of superhydrophobic surfaces by dislocation-selective etching on aluminium, copper and zinc substrates, *Langmuir* **21** 9007-9009 (2005).

<sup>16</sup> Journet C., Moulinet S., Ybert, C., Purcell, S.T., Bocquet, L., Contact angle measurements on superhydrophobic carbon nanotube forests : effect of fluid pressure, *Europhys. Lett.*, **71** 104-109 (2005).